ISSN (Print) 1226-1750
ISSN (Online) 2233-6656
**Journal of Magnetics** 25(4), 556-566 (2020) https://doi.org/10.4283/JMAG.2020.25.4.556

# Research on Denoising Method of Metal Magnetic Memory Signal

**Mingjiang Shi[1]*, Mengfei Zhang[1], Li Gu[2], Zhiqiang Huang[1], Lin Feng[1], and Qing Liu[3]**

*[1]School of Mechatronic Engineering, Southwest Petroleum University, Chengdu 610500, China*
*[2]Southwest Pipeline Company, Chengdu 610500, China*
*[3]Karamay Jianye Energy Co., Ltd., Karamay 834000, China*

(Received 9 September 2020, Received in final form 2 December 2020, Accepted 3 December 2020)

**As the main transportation mode of oil and gas, oil and gas pipelines play an irreplaceable role in energy transportation. Metal magnetic memory detection technology can detect early stress concentration and invisible damage, and can be detected under the action of the geomagnetic field, without the need to magnetize the pipeline in advance. Since the magnetic memory signal is relatively weak, the actual detected signal will be affected by environmental noise, sensor jitter, and pipeline surface deposits. Therefore, the magnetic memory signal needs to be denoised. In this paper, the translation invariant wavelet denoising method, which is improved based on wavelet threshold denoising method, is used to denoise the collected pipeline magnetic memory signals. The experimental results show that the signal-to-noise ratio (SNR) obtained by this method is 4.97 % higher than the unmodified wavelet threshold denoising, and 3.18 % higher than the SNR obtained by the particle swarm optimization wavelet threshold denoising.**

**Keywords :** pipeline defect, stress, weak magnetic detection, magnetic memory signal, simulation

## 1. Introduction

When oil and gas pipelines are affected by the working medium and the environment during processing and manufacturing, factory pressure test or in the service operation, stress concentration will be caused at the defects of the pipeline [1, 2]. At present, Ultrasonic Inspection, Magnetic Flux Leakage Detection, Radiographic Inspection and other Nondestructive Testing methods are often used to realize defect detection, but these methods can only detect the macroscopic damage that has occurred in oil and gas pipelines, and cannot detect the defects caused by early stress concentration. Metal magnetic memory detection technology can detect early stress concentration and invisible damage, and can be detected under the action of the geomagnetic field, without the need to magnetize the pipeline in advance [3, 4]. In actual field applications, metal magnetic memory signals are often interfered by external magnetic fields, and the signals will be influenced with noise. In particular, magnetic memory signals are relatively weak and are easily interfered by noise or even submerged by noise. In fact, the waveform of the detected magnetic memory signal is quite different from the theoretically derived waveform, and the characteristics of the magnetic memory signal cannot be extracted, which greatly affects the detection result. Therefore, the denoising processing of the magnetic memory detection signal is particularly important. The magnetic memory signal is a very weak signal generated in the stress concentration area or defect, which is slightly larger than the geomagnetic field; And the generated magnetic memory signal has random non-stationary characteristics, so it is necessary to find a suitable denoising method to effectively process this signal. Compared with other denoising methods, wavelet analysis has the characteristics of multi-resolution analysis, and can characterize the characteristics of magnetic memory signals in both the time domain and the frequency domain [5]. Therefore, wavelet transform can be used to denoise the magnetic memory signal.

## 2. Method principle

### 2.1. Wavelet transform

For any function, its Fourier transform satisfies the admissible condition [6, 7]:


*Corresponding author: Tel: +86-28-8303-7203
Fax: +86-28-8303-7203, e-mail: swpushi@126.com

$$C_\psi = \int_R \frac{|\psi(\omega)|^2}{|\omega|} d\omega < \infty \tag{1}$$

Then $\psi(t)$ is a mother wavelet or base wavelet, and the mother wavelet is stretched and translated to get:

$$\psi_{a,\tau}(t) = \frac{1}{\sqrt{|a|}} \psi(\frac{t-\tau}{a}) \tag{2}$$

Where, $a$ represents the contraction-expansion factor, $a \in R, a \neq 0$; $\tau$ represents the translation factor, $\tau \in R$, and the wavelet basis function must meet the following conditions [8]:

(1) $\psi(t) \in L^2(R)$ is unitized, that is, $\int_{-\infty}^{+\infty} |\psi(t)|^2 dt = 1$;

(2) $\psi(t) \in L^2(R)$ is a bounded function, that is $\int_{-\infty}^{+\infty} |\psi(t)| dt < \infty$;

(3) The average value of $\psi(t)$ is zero, that is, $\int_{-\infty}^{+\infty} \psi(t) dt = 0$.

Set the function $f(x) \in L^2(R)$, the wavelet transform of this function is the inner product of $f(x)$ and the wavelet basis function [9]:

$$\begin{aligned} W_f(a,\tau) &= < f(t), \psi_{a,\tau}(t) > \\ &= |a|^{-\frac{1}{2}} \int_R f(t) \overline{\psi(\frac{t-\tau}{a})} dt \end{aligned} \tag{3}$$

Recovering from wavelet transform $W_f(a,\tau)$ to the original signal is called inverse wavelet transform:

$$f(t) = \frac{1}{C_\psi} \int_{-\infty}^{+\infty} \int_{-\infty}^{+\infty} \frac{1}{a^2} W_f(a,\tau) \psi(\frac{t-\tau}{a}) da d\tau \tag{4}$$

If the contraction-expansion factor and translation factor are discretized, a discrete wavelet function can be obtained:

$$\begin{aligned} \psi_{j,k} &= \frac{1}{\sqrt{a_0^j}} \psi(\frac{t - k a_0^j \tau_0}{a_0^j}) \\ &= a_0^{-j/2} \psi[a_0^{-j}(t - k a_0^j \tau_0)] \\ &= a_0^{-j/2} \psi(a_0^{-j} t - k\tau_0) \end{aligned} \tag{5}$$

From the discrete wavelet basis function, the discrete wavelet transform can be obtained as:

$$\begin{aligned} WT_f(j,k) &= < f(t), \psi_{j,k}(t) > \\ &= \int_{-\infty}^{+\infty} f(t) \overline{\psi_{j,k}(t)} dt \\ &= a_0^{-j/2} \int_{-\infty}^{+\infty} f(t) \psi(a_0^{-j} t - k\tau_0) dt \end{aligned} \tag{6}$$

### 2.2. Wavelet threshold denoising

There are three classic methods for common wavelet denoising methods: including wavelet threshold denoising method, wavelet coefficient correlation denoising method and modulus maximum method denoising. Among them, wavelet threshold denoising has been widely used in the field of signal and image denoising, which includes hard threshold denoising and soft threshold denoising.

Suppose the one-dimensional signal is $f(n) = s(n) + \sigma \times e(n)$, where $s(n)$ is the useful signal, $e(n)$ is the noise signal, $\sigma$ is the noise intensity, and $f(n)$ is the noisy signal.

Perform discrete wavelet transform on $f(n) = s(n) + \sigma \times e(n)$. Because of the linear nature of wavelet transform, $\omega_{j,k}$ obtained after discrete wavelet transform can be composed of two parts [10], as shown in formula (7):

$$\omega_{j,k} = u_{j,k} + v_{j,k} \tag{7}$$

Where $u_{j,k}$ is the wavelet transform coefficient of the useful signal $s(n)$, and $v_{j,k}$ is the wavelet transform coefficient of the noise signal.

The specific process of wavelet threshold denoising is [11]:

(1) Choose a wavelet function, and determine the decomposition layer number N of wavelet transform, and perform discrete wavelet transform on the noisy signal $f(n) = s(n) + \sigma \times e(n)$ to obtain the wavelet decomposition coefficient $\omega_{j,k}$ of the noisy signal.

(2) Choose an appropriate threshold and threshold the wavelet coefficients obtained in the first step.

(3) Finally, the wavelet coefficients obtained after processing are reconstructed by the inverse wavelet transform to obtain the denoised signal.

### 2.3. Particle swarm algorithm

Particles are used to simulate individual birds, and each particle can be regarded as a potential optimal solution in the N-dimensional search space. Particles have only two

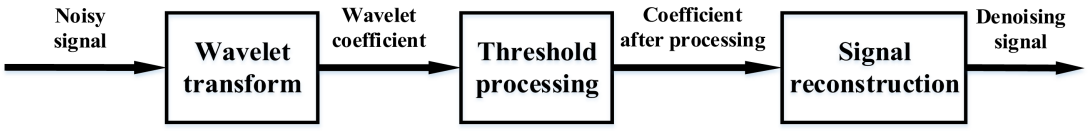


**Fig. 1.** Wavelet threshold denoising process.

attributes: speed and position. Speed represents the speed of movement, and position represents the distance of the particle from the optimal solution. The flight process of the particle is the optimization process of the individual, and the flight speed and individual position of the particles can be dynamically adjusted according to the optimal position of the particle and the optimal position of the swarm. The optimal fitness of each particle is called the individual extremum, and the optimal fitness of all particles in the swarm is called the group extremum [12].

Assume that the search space of particles is D-dimensional space, and the particle swarm is $X=(X_1, X_2, X_3, ...X_n)$. Among them, the D-dimensional vector $X_i=(x_{i1}, x_{i2}, x_{i3},...,x_{iD})$ of the i-th particle represents the position of the particle and also represents a potential optimal solution, and then the fitness value of each particle is calculated according to the fitness function. The speed of individual particles is a D-dimensional vector $V_i(V_{i1}, V_{i2}, V_{i3},...,V_{iD})$, the best fitness value of each particle, that is, the individual extreme value is set to $P_i=(P_{i1}, P_{i2}, P_{i3},...P_{in})$, and the group extreme value of all particles is $P_g=(P_{g1}, P_{g2}, P_{g3},...P_{gn})$. In each iteration of the particle swarm optimization algorithm, the particle updates its position and speed by updating the single best position $P_i$ and the global best position $P_g$.

During each update iteration of the particle swarm optimization algorithm, the speed and position of the particles are updated based on the current individual extreme and the group extreme. The speed update formula and position update formula are formulas (8) and (9) [13]:

$$V_{id}^{k+1}=V_{id}^{k}+c_1r_1(P_{id}^{k}-X_{id}^{k})+c_2r_2(P_{gd}^{k}-X_{id}^{k}) \tag{8}$$

$$X_{id}^{k+1}=X_{id}^{k}+V_{id}^{k+1} \tag{9}$$

The most likely area to obtain the final optimal solution. The first part of formula (8) is called the memory term, which represents the influence of the magnitude and direction of the previous speed; the second part of formula (8) is called the self-cognition term, which is a vector from the current point to the best point of the particle itself, which means that the movement of the particles comes from their own experience; the third part of formula (8) is called the group cognition item, which is a vector from the current point to the best point of the population, reflecting the cooperation and knowledge sharing between particles. Particles use their own experience and the best experience of their companions to determine the next movement. Based on the two formulas (8), (9), a standard form of PSO is formed.

Among them, $i$ represents the i-th particle, $i$ = 1, 2, 3,..., $n$; $d$ = 1, 2, 3,..., $D$; $k$ is the current iteration number; $V_{id}$ is the velocity of the particle; $c_1$ and $c_2$ are non-negative constants, $c_1$ reflects the influence of the best position in the particle flight process on the particle flight speed, $c_2$ reflects the influence of the best position in the entire particle swarm on the particle flight speed; $r_1$ and $r_2$ are random numbers between 0 and 1.

If the objective function is $f(x)$, then the individual extreme update formula of the particle is formula (10):

$$P_i(k+1)=\begin{cases} P_i(k), f(x_i(k+1))\geq f(x_i(k)) \\ P_i(k+1), f(x_i(k+1))\leq f(x_i(k)) \end{cases} \tag{10}$$

The group extremum of the particle swarm is the smallest fitness value among all particles.

The inertia weight $\omega$ is added to the speed update formula of the particle swarm algorithm, so that the particle swarm algorithm has been further optimized. The inertia weight is a non-negative constant, which can balance the local search ability and global search ability of the entire algorithm, and prevent the algorithm from falling into the local optimum. The formula after adding the inertia weight is shown in (11):

$$V_{id}^{k+1}=\omega V_{id}^{k}+c_1r_1(P_{id}^{k}-X_{id}^{k})+c_2r_2(P_{gd}^{k}-X_{id}^{k}) \tag{11}$$

The sym8 wavelet is selected as the wavelet basis function, and the metal magnetic memory signal is subjected to 5-layer wavelet decomposition. In the metal magnetic memory denoising problem, the objective function is the mean square error MSE of the signal. The smaller the objective function value, the better the fitness value:

$$MSE=\frac{1}{N}\sum_{i=1}^{N}(f(i)-f'(i))^2 \tag{12}$$

The specific steps of using particle swarm optimization algorithm to optimize the wavelet threshold are as follows:

Step 1 Initialize the particle swarm, set the dimension of the particle swarm to the number of wavelet decomposition layers, and initialize the particle position and velocity.

Step 2 Assign particles to each layer of high-frequency wavelet coefficient denoising threshold in turn.

Step 3 Run the wavelet denoising program.

Step 4 Calculate the fitness value and use the mean square error of the reconstructed signal as the fitness function to calculate the fitness value of each particle.

Step 5 Evaluate the individual extreme and global extreme of the particle. If the current fitness value is better than the previous fitness value, replace the previous fitness value.

Step 6 Update the speed and position of each particle.

If the termination condition or the maximum number of

iterations is reached, stop the iteration to output the best threshold, otherwise repeat steps 2-6.

### 2.4. Translation invariant wavelet denoising

After the wavelet threshold method denoises the metal magnetic memory signal, it achieves better results, and retain the characteristics of the original signal. However, due to the localized characteristics of wavelet transform, the denoised metal magnetic memory signal will appear pseudo-Gibbs phenomenon at the discontinuous points (singular points) of the signal, which will reduce the denoising effect of the signal. Translation-invariant (TI) wavelet denoising is a denoising method improved on the basis of wavelet threshold denoising. This method can suppress the pseudo-Gibbs phenomenon well; and can improve the SNR of signal, reduce the mean square error.

The pseudo-Gibbs phenomenon is caused by the singular point of the signal, therefore, the main principle of TI wavelet denoising is to change the position of signal discontinuities by the translation signal. Since a signal may have many singular points, each singular point will interfere with each other, therefore, perform n-cycle translation on the signal with noise; then perform wavelet threshold denoising on the translated signal; at last, perform the opposite translation on the denoised signal to obtain the denoised signal.

Assume that a noisy signal is $x_t(0 \le t \le n)$, let $S_h$ represent the time-domain cyclic translation of $h$ ($h$ is a positive integer) on the noisy signal, and the translated signal [14, 15] is shown in the formula (13):

$$(S_h x)_t = x_{(t+h)\bmod_n} \tag{13}$$

$T$ represents the wavelet threshold denoising, and the signal after denoising is represented by $T(S_h x)$. Let $S_{-h}$ represent the reverse cyclic translation, $S_{-h}(T(S_h x))$ represent the signal after wavelet threshold denoising, and let $H_n = \{h : 0 \le h < n\}$. Then the TI wavelet denoising can be expressed as formula (14):

$$\overline{T}(x;(S_h)_{h\in H_n}) = Ave_{h\in H_n} S_{-h}(T(S_h x)) \tag{14}$$

Among them, *Ave* means averaging, and $\overline{T}(x;(S_h)_{h\in H_n})$ is the signal obtained after TI wavelet denoising

The TI wavelet denoising steps for metal magnetic memory signals are as follows:

(1) Input the metal magnetic memory signal, and calculate the translation amount $h$, $h$ = 1, 2, ..., $N$, where $N$ is the signal length.

(2) Use sym8 wavelet basis function to decompose the metal magnetic memory signal with wavelet, and translate the low-frequency signal of each layer obtained after the decomposition; put the coefficients obtained from each level of decomposition into the TI list. When the next level is decomposed, the coefficients in the table of TI are updated until the last 5 levels of decomposition.

(3) Use a fixed threshold (Sqtwolog) for soft threshold denoising.

(4) Reconstruction of metal magnetic memory signal. At each decomposition layer, extract the wavelet coefficients in the TI table, and perform the inverse wavelet transform reconstruction of periodic extension, the low-frequency coefficients reconstructed from each layer update the first column in the TI table until the final restructured metal magnetic memory signal.

## 3. Signal Denoising Simulation

### 3.1. Wavelet threshold denoising

In actual field applications, metal magnetic memory signals are often interfered by external magnetic fields, and the signals will be doped with noise. In particular, magnetic memory signals are relatively weak and are easily disturbed by noise or even submerged by noise. In fact, the waveform of the detected magnetic memory signal is quite different from the theoretically derived waveform, and the characteristics of the magnetic memory signal cannot be extracted, which greatly affects the detection result. Therefore, some random noise is added to the magnetic memory signal for simulation.

In this paper, the pure signal obtained by simulation is added to noise to obtain a noisy signal with a SNR of 5

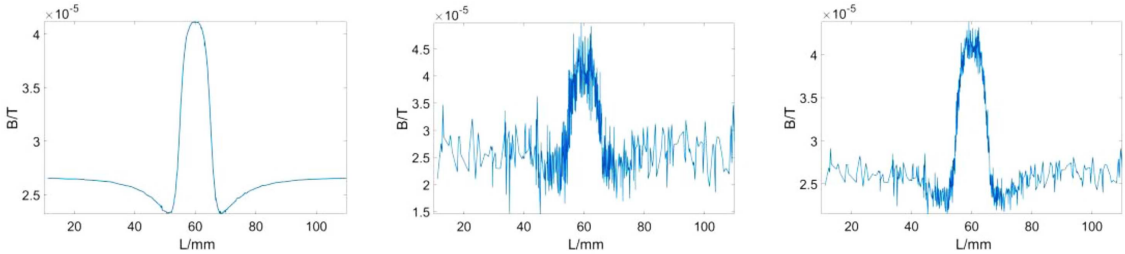


(a) Original standard signal (b) noisy signal (SNR=5) (c) noisy signal (SNR=15)

**Fig. 2.** (Color online) Reference signal: (a) Original standard signal; (b) noisy signal (SNR=5); (c) noisy signal (SNR=15).

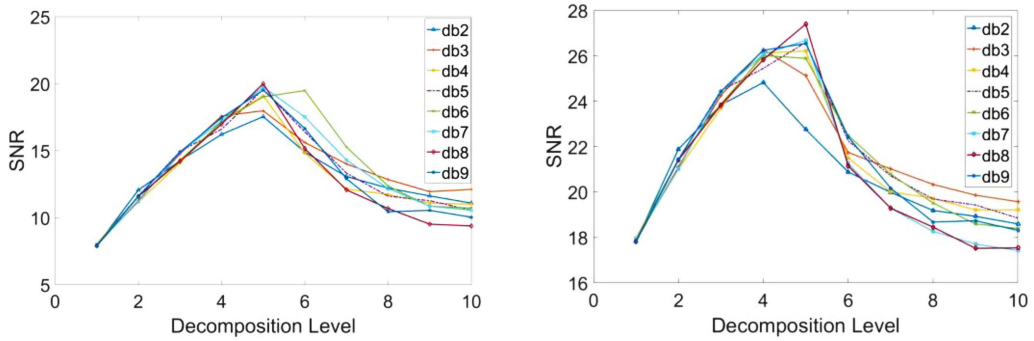


(a) Before denoising (SNR=5) (b) Before denoising (SNR=15)

**Fig. 3.** (Color online) Denoising effect of db wavelet with different decomposition layers and vanishing moments: (a) Before denoising (SNR=5); (b) Before denoising (SNR=15).

and 15 respectively, as shown in Fig. 2.

In order to obtain the optimal wavelet basis function, the number of decomposition layers and the method of threshold selection; The following methods are adopted: first, the commonly used dubechies series wavelets and symlets series wavelets, which are commonly used and suitable for metal magnetic memory signals, are respectively decomposed by 1 to 10 layers of wavelet, then wavelet threshold denoising is performed, and finally perform the reconstruction. Compare and analyze the SNR of db2~db9, Sym2~Sym9 and different decomposition layers, and select the wavelet basis function and decomposition layer with the optimal denoising effect.

The simulation obtained by db2~db9, and the SNR with the decomposition layer number of 1~10 is shown in Fig. 3 and Table 1. It is seen from the Figure that different db wavelets correspond to different SNR. And as the number of decomposition layers increases, the SNR will first increase and then decrease.

It is seen from Fig. 3 that the denoising effect is best when the wavelet basis function is db8 and the number of decomposition layers is 5 layers.

The simulation obtains sym2~sym9, and the SNR with the decomposition layer number of 1~10 is shown in Fig. 4 and Table 2. It can be seen from the Figure that different sym wavelets correspond to different SNR. And as the number of decomposition layers increases, the SNR will first increase and then decrease.

It is seen from Fig. 4 that the wavelet basis function is sym8 and the number of decomposition levels is 5, the denoising effect is the best.

After experiment and simulation research, the useful

**Table 1.** The optimal denoising effect of db wavelet basis functions with different vanishing moments.

| | db2 | db3 | db4 | db5 | db6 | db7 | db8 | db9 |
|---|---|---|---|---|---|---|---|---|
| SNR=5 | 17.5407 | 17.9769 | 19.1048 | 19.5878 | 18.9004 | 19.7613 | 20.0054 | 19.5247 |
| SNR=15 | 22.1068 | 24.3820 | 26.1292 | 26.5899 | 25.8333 | 26.6840 | 27.3073 | 26.5396 |

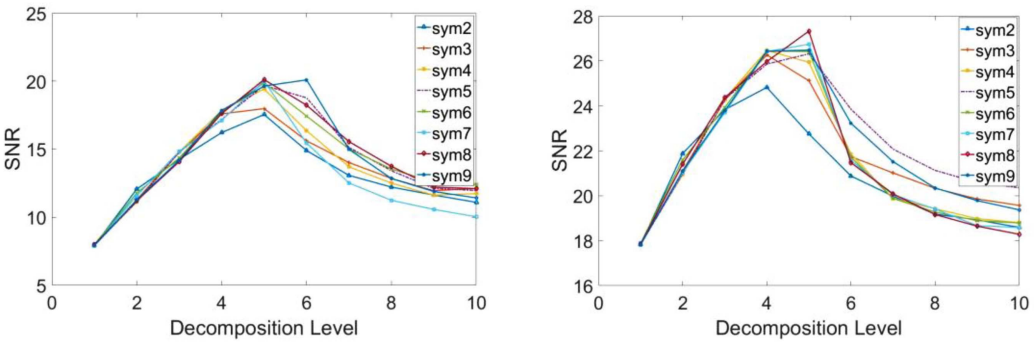


(a) Before denoising (SNR=5) (b) Before denoising (SNR=15)

**Fig. 4.** Denoising effect of sym wavelet with different decomposition layers and vanishing moments: (a) Before denoising (SNR=5); (b) Before denoising (SNR=15).

**Table 2.** The optimal denoising effect of sym wavelet basis functions with different vanishing moments.

| | sym2 | sym3 | sym4 | sym5 | sym6 | sym7 | sym8 | sym9 |
|---|---|---|---|---|---|---|---|---|
| SNR=5 | 17.5407 | 17.9769 | 19.4145 | 19.6831 | 19.8796 | 20.0039 | 20.1177 | 19.6397 |
| SNR=15 | 22.7517 | 25.1177 | 25.9371 | 26.3160 | 26.4192 | 26.7421 | 27.3234 | 26.4797 |

signal of the metal magnetic memory signal is mainly concentrated in the low frequency band, and the noise is mainly high frequency noise. After denoising the magnetic memory signal through the 2-layer and 3-layer decomposition threshold, there is still noise component; after 4-layer decomposition, there is almost no noise component. When the number of decomposition layers is 5, the SNR after denoising is improved. When the number of decomposition layers is higher than 5 layers, the SNR will decrease and useful components will be filtered out. Therefore, the noise of the metal magnetic memory signal is mainly concentrated in the results of the first 4 decomposition scales. In this paper, the number of decomposition layers is selected as 5 layers when performing wavelet threshold denoising. For the selection of wavelet basis function, it can be seen through simulation that, Whether it is a metal magnetic memory signal with a SNR before denoising SNR=5 or SNR=15, the sym8 wavelet basis function has the best denoising effect, the highest SNR, and the most similar to the original signal.

### 3.2. Particle swarm optimization wavelet threshold denoising

The particle swarm optimization (PSO) algorithm is used to optimize the wavelet threshold and then denoise the noisy metal magnetic memory signal. The denoised SNR and the mean square error of the signal are used as indicators to measure the wavelet threshold denoising effect of the PSO algorithm.

Because the number of decomposition layers is 5, the particle dimension is 5; the particle swarm size is 100, and the maximum number of iterations is 100; the learning factors $c_1$ and $c_2$ are both set to 2; the inertia weight $\omega$ is set to 0.6. Fig. 5 and 6 are comparison diagrams between the optimized results and other threshold selection rules.

It is seen from Table 3 that among the commonly used threshold selection rules, the general threshold selection rule has the best denoising effect on magnetic memory signals, while the PSO wavelet threshold denoising effect is better, and the PSO wavelet threshold denoising method

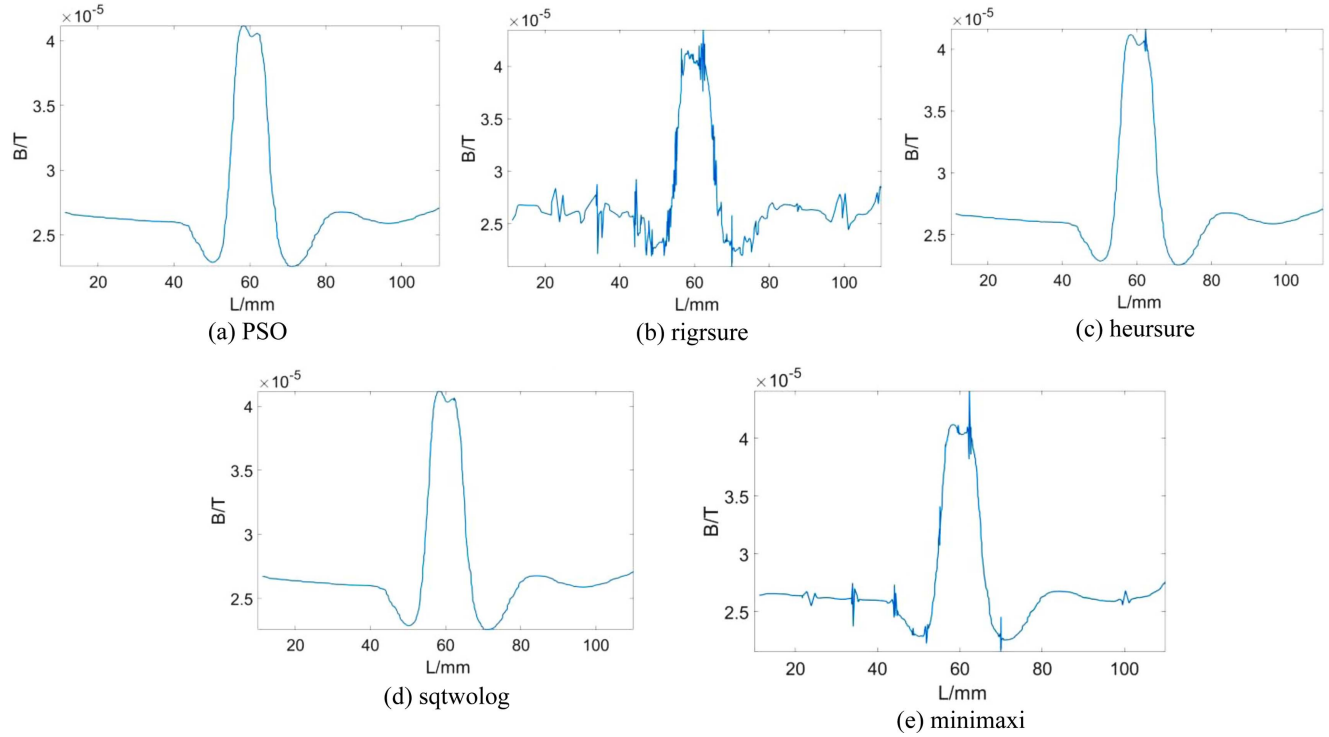


**Fig. 5.** (Color online) Denoising effect diagram of magnetic memory signal (SNR=5) with different threshold selection rules: (a) PSO; (b) rigrsure; (c) heursure; (d) sqtwolog; (e) minimaxi.

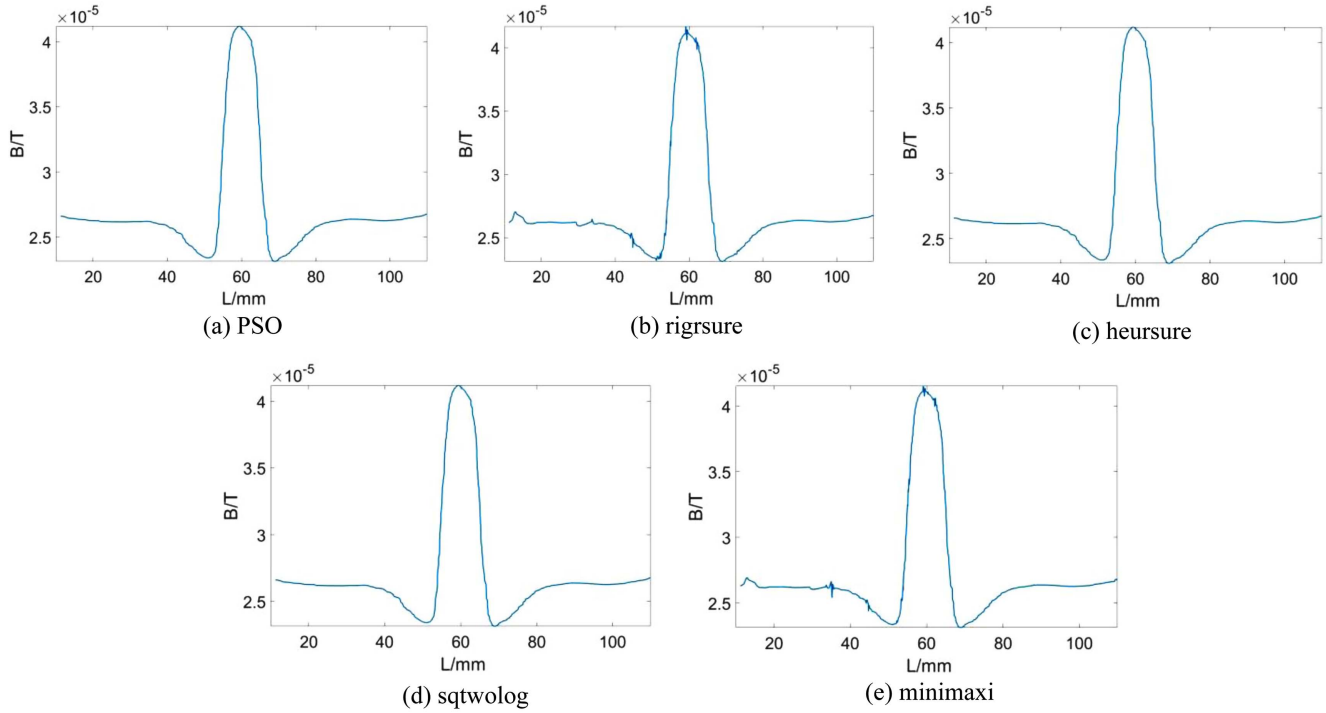


**Fig. 6.** (Color online) Denoising effect diagram of magnetic memory signal (SNR=15) with different threshold selection rules: (a) PSO; (b) rigrsure; (c) heursure; (d) sqtwolog; (e) minimaxi.

**Table 3.** SNR of different threshold selection methods after denoising.

| Wavelet threshold selection method | Before denoising (SNR=5) | Before denoising (SNR=15) |
|---|---|---|
| PSO optimized wavelet threshold denoising | 20.1121 | 27.3237 |
| rigrsure | 15.3658 | 26.6456 |
| heursure | 20.0592 | 27.3230 |
| sqtwolog | 20.1117 | 27.3234 |
| minimaxi | 18.8655 | 26.9313 |

is better than the commonly used threshold method. This method improves the SNR, but has little effect.

### 3.3. Translation invariant wavelet denoising

After the wavelet threshold method denoises the metal magnetic memory signal, it can achieve better results and retain the characteristics of the original signal. However, due to the localized characteristics of wavelet transform, the denoised metal magnetic memory signal will appear pseudo-Gibbs phenomenon at the discontinuous points (singular points) of the signal, which will reduce the denoising effect of the signal. TI wavelet denoising is a denoising method improved on the basis of wavelet threshold denoising. This method can well suppress the pseudo-Gibbs phenomenon; and can improve the SNR, reduce the mean square error.

It is seen from Fig. 7 and Fig. 8 and Table 4 that the TI

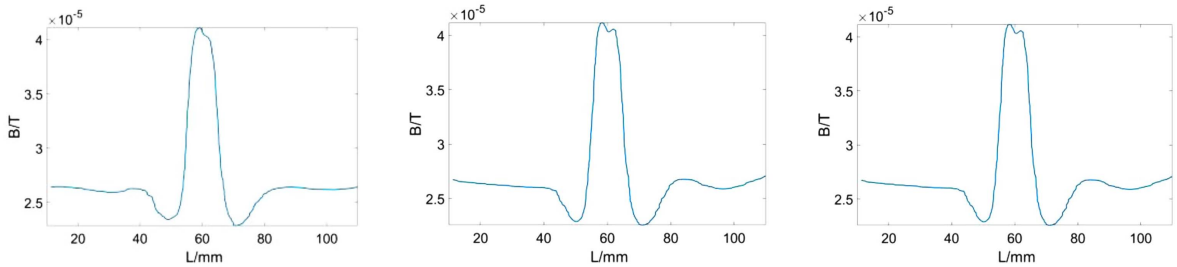


**Fig. 7.** (Color online) Comparison of denoising effects of three methods on noisy signals (SNR=5): (a) TI wavelet denoising; (b) PSO wavelet threshold denoising; (c) Wavelet threshold denoising.

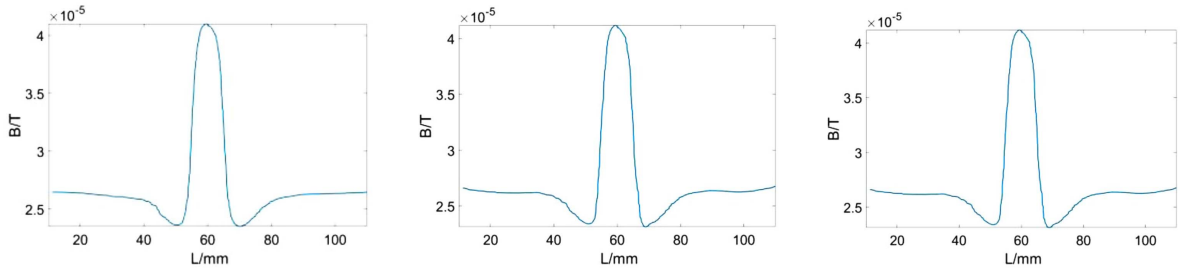


(a) TI wavelet denoising (b) PSO wavelet threshold (c) Wavelet threshold denoising

**Fig. 8.** (Color online) Comparison of denoising effects of three methods on noisy signals (SNR=15): (a) TI wavelet denoising; (b) PSO wavelet threshold denoising; (c) Wavelet threshold denoising.

**Table 4.** Comparison of three denoising methods.

| SNR before denoising | TI wavelet denoising | PSO wavelet threshold denoising | Wavelet threshold denoising |
|---|---|---|---|
| | SNR | SNR | SNR |
| SNR=5 | 20.7236 | 20.1121 | 20.1117 |
| SNR=15 | 27.5830 | 27.3237 | 27.3234 |

wavelet threshold denoising has a higher SNR and a smaller root mean square error than the wavelet threshold denoising method. Among them, for the magnetic memory signal with SNR=5 before denoising, the SNR is increased by 3.04 %, and the mean square error is reduced by 6.80 %; for the noisy magnetic memory signal with SNR=15 before denoising, The SNR is increased by 0.09 %, and the mean square error is reduced by 2.94 %.

The new threshold function with parameters can overcome the shortcomings of the wavelet threshold function denoising method, adjust the parameters to make it have the advantages of both hard and soft threshold functions. And add a smooth transition zone within the critical threshold, which can retain a portion of useful high-frequency signals during threshold processing, and can better suppress the overkill of detail coefficients and signal oscillation. For random noisy signals, the parameterized wavelet threshold function method based on PSO optimization can be used to automatically optimize the parameters of the threshold function, determine the best wavelet basis function and the number of decomposition layers, and obtain the best denoising effect. The TI wavelet denoising method can better remove the pseudo Pseudo-Gibbs phenomenon in signal denoising, has better visual effects, and can reduce the root mean square error between the original signal and the estimated signal, and improve the signal noise In comparison, the denoising effect on magnetic memory signals is also better than the previous two denoising methods.

## 4. Metal Magnetic Memory Signal Experiment and Denoising

Where the defects and stresses of the pipeline are concentrated, a leakage magnetic field is formed. The state of magnetic charge accumulation determines the direction of the leakage magnetic field, and the internal magnetic domain structure determines the strength of the leakage magnetic field [16]. When the pipeline is under the combined action of the geomagnetic field and the working load, the magnetic domains inside the pipeline will be irreversibly reoriented due to magnetostriction. The stress concentration area forms a leakage magnetic field, the tangential component p of the leakage magnetic field has a maximum value, and the normal component s changes sign and has a zero point [17-19]. The detection principle is shown in Fig. 9.

The magnetic memory detection system includes fluxgate sensor, signal processing circuit includes frequency selecting amplifier, phase sensitive detector, Analog-to-digital converter A/D and CPU controller, and upper computer.

In magnetic memory detection, the quality of the sensor and its range and characteristics are very important to the detection results, and it is the most important part of the instrument. In magnetic memory testing equipment, magnetic sensor is used to measure the size and distribution of

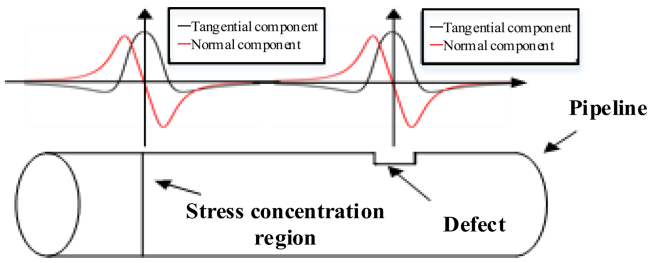


**Fig. 9.** (Color online) Principle diagram of magnetic memory detection.

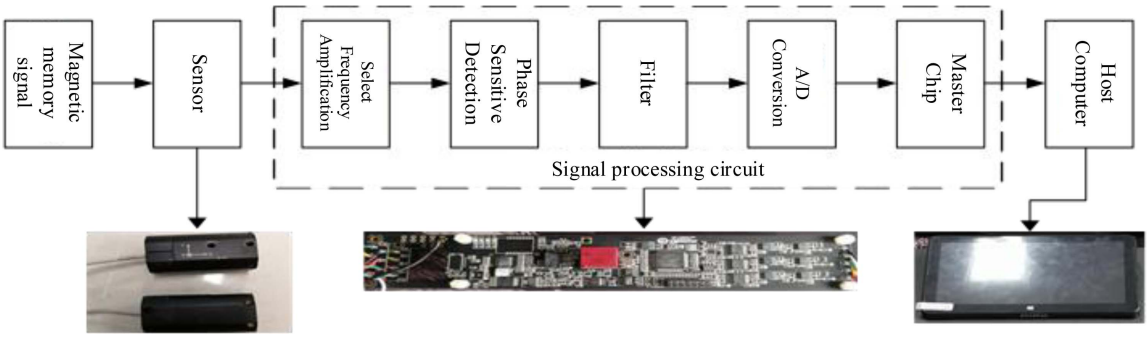


**Fig. 10.** (Color online) Magnetic memory detection system.

magnetic field on the surface of pipeline to be tested.

The metal magnetic memory signal detection system for oil and gas pipelines is shown in Fig. 10. Since the magnetic memory signal is a weak magnetic field, the strength of the magnetic field with the earth is an order of magnitude, and the detection requires high accuracy. A three-axis fluxgate sensor is used. The output of the fluxgate sensor is mainly the fundamental wave signal with the same frequency as the sensor excitation signal and various harmonic components. The useful signal is the second harmonic component, and the fundamental wave and other harmonic components are noise signals. Therefore, it needs to go through a frequency selective amplifier circuit to amplify the second harmonic and suppress the fundamental wave and other harmonic components. The magnetic memory signal after the frequency selective amplifier circuit still contains part of the fundamental wave and other harmonic component noise, so the phase-sensitive detection circuit is indispensable, and the phase-sensitive detection circuit can almost completely eliminate other harmonic components. After the previous frequency selective amplification and phase-sensitive detection circuit, the magnetic memory signal can't be directly sampled. At this time, the signal is a pulse signal, which is similar to a sawtooth wave. Therefore, smooth filtering is required to smooth the signal and filter out the pulsation component. Finally, it enters the main control chip after A/D sampling, converts the voltage signal into a magnetic field signal and sends it to the host computer through the serial port.

When the metal magnetic memory signal is collected in real time, the magnetic memory signal collected by the two fluxgate sensors passes through the signal processing circuit and is converted to the host computer after A/D conversion. The host computer saves the original signal to the corresponding folder. On the other hand, the magnetic

**Table 5.** Chemical composition of experimental pipeline (mass fraction, %).

| Chemical composition | Mn | Si | C | Cr | Ni | Cu | P | S |
|---|---|---|---|---|---|---|---|---|
| No. 20 steel | 0.35~0.65 | 0.17~0.37 | 0.17~0.23 | ≤ 0.25 | ≤ 0.30 | ≤ 0.25 | ≤ 0.035 | ≤ 0.035 |

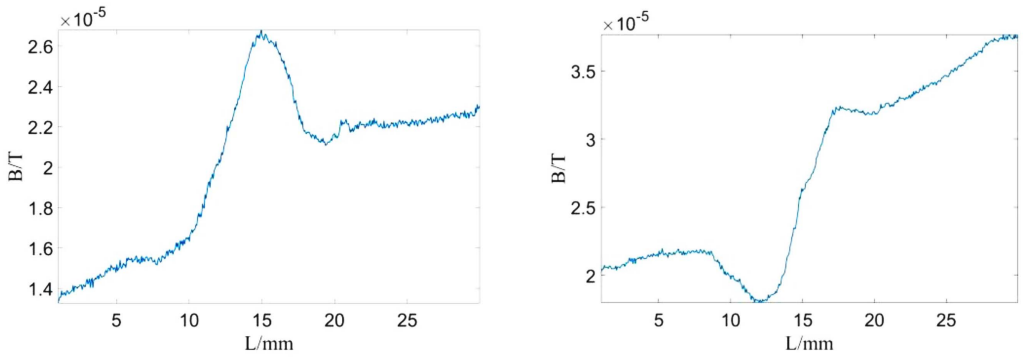


(a) Actual tangential signal (b) Actual normal signal

**Fig. 11.** (Color online) Actual magnetic memory signal: (a) Actual tangential signal; (b) Actual normal signal.

memory signal will be displayed in real time. If it encounters obstacles or cannot continue to collect signals, it will pause and mark the cause of the failure.

The pipe material used in this paper is No. 20 steel, and its mechanical properties and chemical composition are shown in Table 5:

In the research of quantitative inversion of defect size based on metal magnetic memory, it is necessary to obtain defect magnetic memory data of different sizes to extract signal features for support vector machine training and inversion. The pipe used in this experiment is a pipe with a diameter of 80 mm and a wall thickness of 7 mm. The defect is designed with a radius of 12 mm and a depth of 5 mm.

The metal magnetic memory signal collected on site is affected by probe jitter, measurement noise, pipeline surface deposits, and external magnetic field interference, and the signal is doped with noise. In fact, the waveform of the detected magnetic memory signal is quite different from the theoretically derived waveform, and the charac-

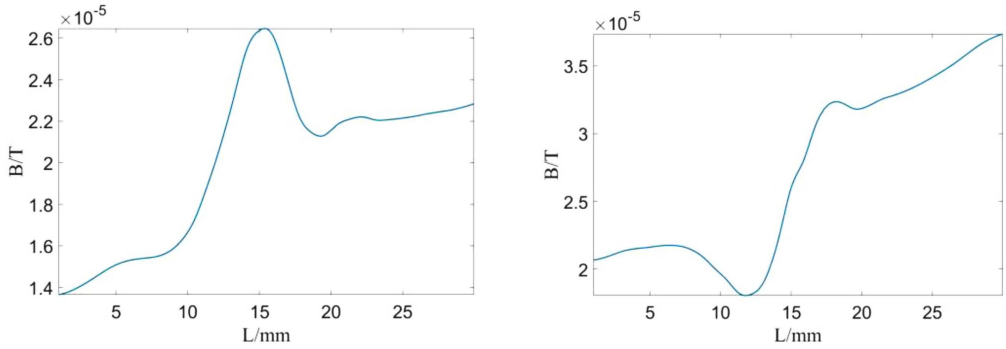


(a) Tangential signal (b) Normal signal

**Fig. 12.** (Color online) Magnetic memory signal after wavelet threshold denoising: (a) Tangential signal; (b) Normal signal.

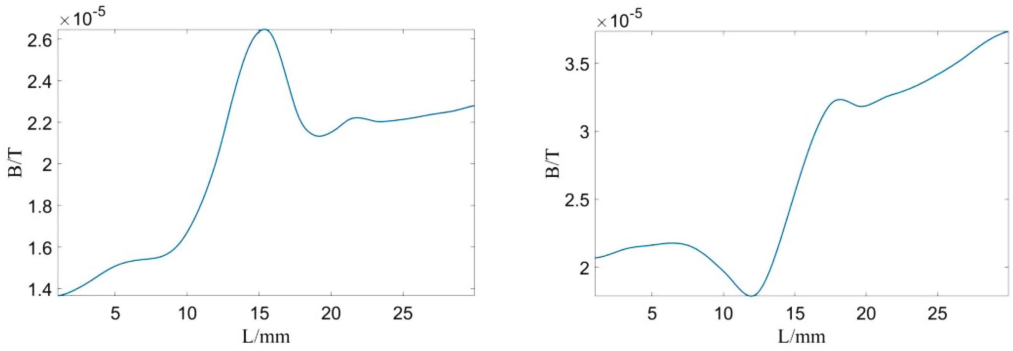


(a) Tangential signal (b) Normal signal

**Fig. 13.** (Color online) Magnetic memory signal after PSO wavelet threshold denoising: (a) Tangential signal; (b) Normal signal.

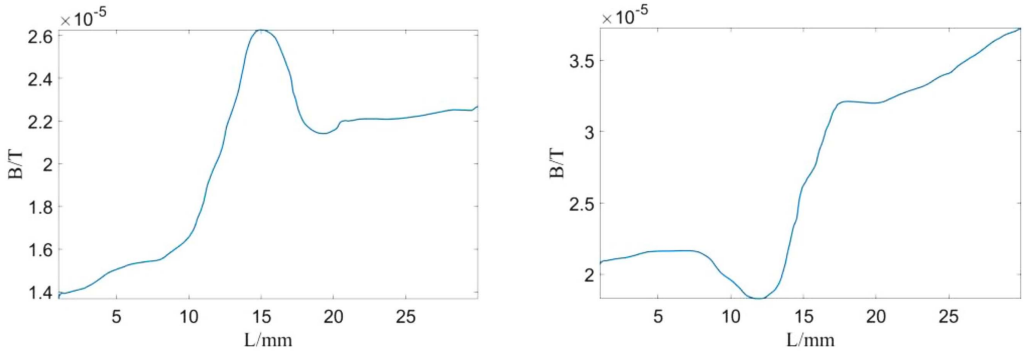


(a) Tangential signal (b) Normal signal

**Fig. 14.** (Color online) Magnetic memory signal after TI wavelet denoising: (a) Tangential signal; (b) Normal signal.

**Table 6.** Denoising effects of three methods on actual magnetic memory signals.

| Magnetic memory signal | Wavelet threshold denoising | PSO wavelet threshold denoising | TI wavelet denoising |
|---|---|---|---|
| | SNR | SNR | SNR |
| Tangential signal | 23.5101 | 24.0190 | 24.5170 |
| Normal signal | 27.1682 | 28.6744 | 29.2865 |

teristics of the magnetic memory signal cannot be extracted, which greatly affects the detection result. The magnetic memory signal is shown in Fig. 11:

The result of ordinary wavelet threshold denoising is shown in Fig. 12:

The result of PSO wavelet threshold denoising is shown in Fig. 13:

The result of TI wavelet denoising is shown in Fig. 14:

It is seen from Table 5 that the TI wavelet denoising has a better denoising effect on metal magnetic memory signals than ordinary wavelet threshold denoising. The SNR after denoising the tangential component of the magnetic memory signal is improved by 2.07 % compared with the PSO wavelet threshold denoising, and 4.28 % higher than the wavelet threshold denoising. The normal component is improved by 2.13 % than the PSO wavelet threshold denoising, and 7.80 % higher than the wavelet threshold denoising. The use of TI wavelet denoising can improve the SNR of magnetic memory signals and obtain more accurate signals.

## 5. Conclusion

Through the metal magnetic memory detection of oil and gas pipeline defects, it was found that the detection signal was seriously interfered by probe jitter, measurement noise, pipeline surface deposits, and external magnetic fields, which seriously affected the subsequent quantitative analysis of defects. The detection signal was denoised by using wavelet threshold denoising, PSO wavelet threshold denoising, and TI wavelet denoising. The comparison shows that the SNR of metal magnetic memory signal denoised by TI wavelet is 4.97 % higher on average than that of wavelet threshold denoising, and is 3.17 % higher on average than that of PSO wavelet threshold denoising.

## Acknowledgments

This work was support by the National Natural Science Foundation of China (Grant: 21204139), the open Fund of Key Laboratory of Oil &Gas Equipment Ministry of Education Southwest Petroleum University (Grant: OGE 201701-03) the State Key Laboratory of Oil and Gas Reservoir Geology and Exploitation (Southwest Petroleum University) (Grant: PLN201829).

## References

[1] Q. Feng, R. Li, B. Nie, B. H. Nie, S. C. Liu, and H. Zhang, Sensors **17**, 1 (2016).
[2] M. J. Shi, Feng L, Z. Q. Huang, Z. Q. Huang, M. F. Zhang, and Qing Liu, J. Magn **24**, 3 (2019).
[3] A. A. Dubov, J. Chem. Petrol. Eng. **47**, 11 (2012).
[4] D. N. Chen, L. Huang, H. Y. Yu, X. C. Zhong, and Z. W. Liu, J. Magn. **24**, 3 (2019) pp 485-490.
[5] M. K. Su, J. S. Zheng, Y. X. Yang, and Q. Wu, GPS Solut **22**, 3 (2018) pp 1-12.
[6] S. G. Mallat, IEEE T Pattern Anal. **11**, **7** (1989).
[7] T. Kumar and U. K. Mandal, Math Method Appl. Sci. **42**, 9 (2019).
[8] P. Jang and G. Choi, IEEE Trans. Magn. **53**, 1 (2017).
[9] T. Abuhamdia, S. Taheri, and J. Burns, J. Vib. Control. **24**, 9 (2018).
[10] X. G. Zhang, Z. J. Zou, H. Guo, and J. C. Yin, Indian J. Geo-Mar. Sci. **46**, 9 (2017).
[11] S. K. Ren, X. Z. Ren, Z. X. Duan, and Y. W. Fu, NDT&E Int. **103**, (2019) pp 77-83.
[12] W. Wang, J. Cao, N. Zhang, J. Lin, and W. Liao, Energy Convers. Manag. **132**, 189 (2017).
[13] A. Altay, G. Kayakutlu, [J]. Lect Notes Eng. Comput. Sci. **2078**, 0958 (2011).
[14] H. S. Choi, I. H. Park, and S. H. Lee, IEEE Trans. Magn. **42**, 663 (2006).
[15] K. S. Xu, K. Yang, J. Liu, and Y. Wang, J. Magn. Magn. Mater **498**(C), (2020).
[16] G. M. Lin, H. Y. Lin, and K. Dong, Adv. Mat. Res. **503-504**, (2012).
[17] D. B. Wu, M. Q. Xu, and J. W. Li, Appl. Mech. Mater **34-35**, 1021 (2010).
[18] D. B. Wu, M. Q. Xu, and H. Y. Xing, Appl. Mech. Mater **34-35**, 1021 (2010) pp 855-858.
[19] N. Chen, H. Lin, and X. K. Wang, J. Magn. Magn. Mater **462**, (2018) pp 144-152.